INTERNATIONAL JOURNAL FOR NUMERICAL METHODS IN FLUIDS, VOL. 14, 961–980 (1992)

SIMULATING TWO-DIMENSIONAL TURBULENT FLOW BY USING THE k–ε MODEL AND THE VORTICITY–STREAMFUNCTION FORMULATION

D. ELKAIM, M. REGGIO AND R. CAMARERO

Department of Applied Mathematics, École Polytechnique de Montréal, CP 6079 Succ. A, Montréal, Québec, Canada H3C 3A7

SUMMARY

A numerical procedure to solve turbulent flow which makes use of the k–ε model has been developed. The method is based on a control volume finite element method and an unstructured triangular domain discretization. The velocity–pressure coupling is addressed via the vorticity–streamfunction and special attention is given to the boundary conditions for the vorticity. Wall effects are taken into account via wall functions or a low-Reynolds-number model. The latter was found to perform better in recirculation regions. Source terms of the k and ε transport equations have been linearized in a particular way to avoid non-realistic solutions. The vorticity and streamfunction discretized equations are solved in a coupled way to produce a faster and more stable computational procedure. Comparison between the numerical predictions and experimental data shows that the physics of the flow is correctly simulated.

KEY WORDS Vorticity–streamfunction Turbulent flow Control volume k–ε model

1. INTRODUCTION

Numerical computation of laminar or turbulent flows requires the solution of a set of non-linear partial differential equations, all of which are of the convection–diffusion type.

As the Reynolds number of the flow increases, the convection terms become more and more dominant and regular Galerkin finite element and centred difference methods lead to spurious oscillations in the solution. To overcome this difficulty, Patankar[1] proposed an interpolation function which is based on the best possible solution of the convection–diffusion equation. This function takes into account the relative strength of the convection and is locally defined in a flow-oriented co-ordinate system. It has the advantage of reducing numerical diffusion and benefits from the easy physical interpretation of control volume methods when applied to unstructured triangular meshes. It was further tested and used successfully[2–4] to simulate a variety of laminar fluid flow and heat transfer problems. Here it is used to simulate turbulent flows as well.

The velocity–pressure coupling can be addressed via either an unequal-order[3] or an equal-order[2] velocity–pressure interpolation[3] or via the vorticity–streamfunction formulation that inherently satisfies the divergence-free constraint.[5,6]

As will be seen later, the vorticity–streamfunction formulation is only approximate for turbulent flows and does not go over well to 3D. Nevertheless, as an intermediate step towards full simulation of the 3D Navier–Stokes turbulent equations in their primitive formulation by a control volume finite element method and in order to gain a better insight of the exponential

0271–2091/92/080961–20$10.00

Received 15 January 1990
Revised 24 June 1990

interpolation function, in this paper we will address the velocity–pressure coupling via the vorticity–streamfunction formulation. The good results of the present calculations will show that the simplifications associated with the formulation for turbulent flows can be accepted as a modelling approximation. The major difficulty becomes associated with the computation of the vorticity on solid walls and this difficulty becomes even more restricting when computing turbulent flows with a k–ε model because of the wall functions usually associated with the use of such a model. In this respect two possible types of boundary conditions, to be imposed on the vorticity on solid walls when a k–ε model is used, have also been investigated.

2. GOVERNING EQUATIONS

The phenomenon under consideration is represented by a steady two-dimensional or axisymmetric laminar or turbulent flow. The governing equations for this system may be divided, for convenience, into two groups, i.e. the fluid motion equations and the turbulence equations.

2.1. Fluid flow equations

The axisymmetric equations representing the conservation of mass and momentum are written via the vorticity–streamfunction formulation (ω, ψ). The vorticity is expressed by

$$\omega = \frac{\partial v}{\partial x} - \frac{\partial u}{\partial y}, \tag{1}$$

where u and v are the velocity components in the x- and y-direction respectively.

The streamfunction ψ is expressed in such a way that the continuity equation is identically satisfied. We then have

$$r\rho u = \frac{\partial \psi}{\partial y}, \qquad r\rho v = -\frac{\partial \psi}{\partial x}, \tag{2}$$

with r the radius for axisymmetric configurations.

Using (1) and (2), the governing equations for the fluid flow problem become[7] for the streamfunction

$$\frac{\partial^2 \psi}{\partial x^2} + \frac{\partial^2 \psi}{\partial y^2} = -\rho \omega r + \left(\frac{1}{r} \frac{\partial \psi}{\partial r} \right) \alpha_{\text{axi}} \tag{3}$$

and for the vorticity

$$\frac{\partial}{\partial x}(r\rho u\omega) + \frac{\partial}{\partial y}(r\rho v\omega) = \frac{\partial}{\partial x}\left(r\mu_e \frac{\partial \omega}{\partial x} \right) + \frac{\partial}{\partial y}\left(r\mu_e \frac{\partial \omega}{\partial y} \right) + \left(r\rho v\omega - \frac{\mu_e \omega}{r} \right) \alpha_{\text{axi}}, \tag{4}$$

where ρ is the density. Also, $\alpha_{\text{axi}} = 1$ and $y = r$ for axisymmetric flow or $\alpha_{\text{axi}} = 0$ and $r = 1$ for planar two-dimensional flow. μ_e is the effective viscosity given by

$$\mu_e = \mu + \mu_t, \tag{5}$$

μ being the laminar viscosity and μ_t the turbulent viscosity evaluated according to the k–ε model of turbulence.[8]

Mention has to be made here of the fact that (4) is not derived from first principles. The derivation of Gosman *et al.*[7] is a gross approximation for the shear stress expression. In fact it is well known[9] that the exact vorticity equation is so complicated as to be impractical for variable viscosity turbulent flows. However, no attempt will be made here to justify their derivation in a

systematic way. Equation (4) will be accepted as a modelling approximation which will prove to be very useful in view of the quality of the numerical predictions when compared to experiments.

2.2. *Turbulence equations*

Turbulence kinetic energy:

$$\frac{\partial}{\partial x}(r\rho uk)+\frac{\partial}{\partial y}(r\rho vk)=\frac{\partial}{\partial x}\left(r\frac{\mu_e}{\sigma_k}\frac{\partial k}{\partial x}\right)+\frac{\partial}{\partial y}\left(r\frac{\mu_e}{\sigma_k}\frac{\partial k}{\partial y}\right)+r(G_k-\rho\varepsilon). \tag{6}$$

Energy dissipation:

$$\frac{\partial}{\partial x}(r\rho u\varepsilon)+\frac{\partial}{\partial y}(r\rho v\varepsilon)=\frac{\partial}{\partial x}\left(r\frac{\mu_e}{\sigma_\varepsilon}\frac{\partial \varepsilon}{\partial x}\right)+\frac{\partial}{\partial y}\left(r\frac{\mu_e}{\sigma_\varepsilon}\frac{\partial \varepsilon}{\partial y}\right)+\frac{r\varepsilon}{k}(c_1G_k-c_2\rho\varepsilon). \tag{7}$$

G_k and c_1G_k are generation terms, as opposed to the destruction terms $-\rho\varepsilon$ and $-c_2\rho\varepsilon$. G_k is given by

$$G_k=\mu_t\left\{2\left[\left(\frac{\partial u}{\partial x}\right)^2+\left(\frac{\partial v}{\partial y}\right)^2\right]+\left(\frac{v}{r}\right)^2\alpha_{axi}+\left(\frac{\partial u}{\partial y}+\frac{\partial v}{\partial x}\right)^2\right\}. \tag{8}$$

The turbulent viscosity is related to k and ε via

$$\mu_t=c_d\rho\frac{k^2}{\varepsilon}. \tag{9}$$

This turbulence model has five constants: $\sigma_k, \sigma_\varepsilon, c_1, c_2$ and c_d. The following values are commonly used:[8]

σ_k	σ_ε	c_1	c_2	c_d
0·9	1·22	1·44	1·92	0·09

In general the k–ε model is only valid in regions where the flow is entirely turbulent. Close to the solid walls viscous effects become dominant and such a model does not lead to acceptable predictions. For numerical computations there are two main methods for treating the adjacent wall regions more carefully: (i) wall functions or the law of the wall and (ii) low-Reynolds-number models.

Law of the wall. The region close to solid walls can be divided into two sublayers (Figure 1): (a) a laminar sublayer or viscous sublayer where purely viscous effects are dominant and (b) a turbulent sublayer. We suppose that the first computational point P adjacent to the wall is in the turbulent sublayer (Figure 2) and that the velocity vector at this point is parallel to the wall. In this sublayer the velocity has a known logarithmic variation.[10] In this case conditions on the wall are related to conditions at point P through this law.

The computational procedure thus skips over the viscous sublayer where many grid points are necessary to adequately describe the steep gradients in this region. It is only necessary to make sure that point P is indeed in the turbulent sublayer. Other types of sublayers can be considered in building the law of the wall,[11] with the point P within any of these sublayers. Naturally the velocity variation has to be changed accordingly.

Here we consider only two sublayers (viscous and turbulent), with the first computational point P being in the turbulent sublayer. Details on how to apply this law of the wall to numerical computations are given in the section dealing with boundary conditions.

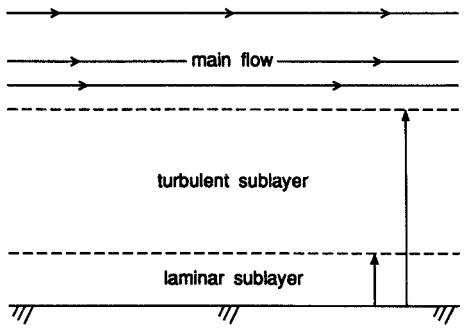

Figure 1. Region close to solid walls

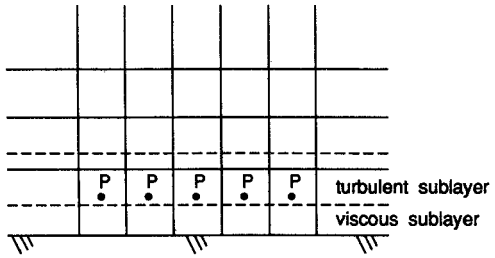

Figure 2. Location of points adjacent to wall

Low-Reynolds-number models. These models use the same basic equations for k and ε, together with damping functions on the viscosity and turbulence equations in order to take into account wall effects. This approach allows calculations to be done up to the solid walls, eliminating the need for a special computational procedure near the boundaries. Various models of this kind exist;[12,13] however, they all have a major disadvantage when compared to the k–ε model with the law of the wall, namely an excessive number of grid points are needed in the sublayers to adequately describe the gradients in these regions. Convergence rates become too slow for realistic computations to be done,[14] particularly when an explicit time-marching solution procedure is applied. Nevertheless, in this work we also used a low-Reynolds-number model to take wall effects into account because in our case an implicit solution procedure was applied, making the convergence rates acceptable. The transport equations for k and ε are[14] (terms in boxes represent the damping functions that are added to the original k–ε model as described by (6)–(9))

$$\frac{\partial}{\partial x}(r\rho uk)+\frac{\partial}{\partial y}(r\rho vk)=\frac{\partial}{\partial x}\left(r\frac{\mu_e}{\sigma_k}\frac{\partial k}{\partial x}\right)+\frac{\partial}{\partial y}\left(r\frac{\mu_e}{\sigma_k}\frac{\partial k}{\partial y}\right)+r(G_k-\rho\varepsilon)-\boxed{2\mu r\left(\frac{\partial k^{1/2}}{\partial y}\right)^2}, \tag{10}$$

$$\frac{\partial}{\partial x}(r\rho u\varepsilon)+\frac{\partial}{\partial y}(r\rho v\varepsilon)=\frac{\partial}{\partial x}\left(r\frac{\mu_e}{\sigma_\varepsilon}\frac{\partial \varepsilon}{\partial x}\right)+\frac{\partial}{\partial y}\left(r\frac{\mu_e}{\sigma_\varepsilon}\frac{\partial \varepsilon}{\partial y}\right)+\frac{r\varepsilon}{k}\left(c_1G_k-c_2\rho\varepsilon\boxed{f_2}\right)+\boxed{2\frac{r\mu\mu_t}{\rho}\left(\frac{\partial^2 u}{\partial y^2}\right)^2}, \tag{11}$$

the constants c_d, c_1, c_2, σ_k and σ_ε and the generation term G_k stay the same as before. The turbulent viscosity is now

$$\mu_t = c_d \boxed{f_\mu} \frac{\rho k^2}{\varepsilon}, \tag{12}$$

where

$$f_\mu = \exp\left(-\frac{3{\cdot}4}{(1+R_t/50)^2}\right), \tag{13}$$

and

$$f_2 = 1{\cdot}0 - \frac{0{\cdot}4}{1{\cdot}8}\exp\left(-\frac{(R_t)^2}{36}\right), \tag{14}$$

where

$$R_t = \frac{\rho k^2}{\varepsilon\mu}. \tag{15}$$

3. BOUNDARY CONDITIONS

On each of the computational domain boundaries conditions are required to solve the differential equations. Generally there are four types of boundaries: inlet, outlet, solid walls and symmetry axis. For each type and for each unknown let us see what boundary conditions are to be specified.

3.1. Boundary conditions for k–ε

Solid walls. If the law of the wall is applied, then we suppose that the first computational point close to the wall is in the turbulent sublayer. At this point the velocity U_p is parallel to the boundary and has a logarithmic variation[10]

$$|U_P| = \frac{u^*}{\kappa}\ln(Ey_p^+); \tag{16}$$

u^*, called the friction velocity, and y_p^+, representing a dimensionless distance from point P (or 'p') to the wall, are defined by

$$u^* = \left(\frac{\tau_w}{\rho}\right)^{0{\cdot}5}, \tag{17}$$

$$y_p^+ = \frac{\rho y_p u^*}{\mu}, \tag{18}$$

where τ_w is the shear stress at the wall, κ is the Von Karman constant, E is a roughness parameter ($\kappa = 0{\cdot}4$, $E = 9{\cdot}7$)[10] and y_p is the actual distance from point P to the wall.

It is the value of the dimensionless distance y_p^+ that sets the limits between the different sublayers. For the turbulent layer y_p^+ is approximately between 10 and 400.[11]

We now suppose that the turbulent sublayer is in local equilibrium so that the rate of k-production is exactly equal to its destruction rate. This leads to

$$\frac{\mu_t}{\rho}\left(\frac{\partial u}{\partial y}\right)^2 = \varepsilon. \tag{19}$$

By further supposing that the shear stress is constant in the sublayer ($\tau_p = \tau_w$) and using the logarithmic law, it is found that

$$k_p = \frac{u^{*2}}{\sqrt{c_d}}, \tag{20}$$

$$\varepsilon_p = \frac{u^{*3}}{\kappa y_p}. \tag{21}$$

Equations (20) and (21) give the values of k and ε at point P without solving the transport equations (6) and (7). In order to obtain u^*, equations (16) and (18) are combined to yield the non-linear equation:

$$|U_P| = \frac{u^*}{\kappa} \ln\left(\frac{E\rho y_p u^*}{\mu}\right). \tag{22}$$

The velocity U_P is known from the solution of the vorticity and streamfunction transport equations (3) and (4). The values of k_p and ε_p are used to calculate the turbulent viscosity and serve as boundary conditions (Dirichlet) for the rest of the domain (Figure 3). It is not necessary to calculate k and ε at the walls. The viscosity there is equal to the laminar viscosity.

When the low-Reynolds-number model is used, the turbulence kinetic energy is set to zero on the solid walls because there are no velocity fluctuations (no-slip condition $u = v = 0$) on this type of boundary. The dissipation ε is also set equal to zero, although the justification for this is less straightforward than for k (see Reference 15 for a full explanation).

Inlet. Values of k and ε are not known at the inlet but, if they are not given by experimental data, some reasonable assumptions can be made. The kinetic energy of turbulence is estimated according to a certain percentage of the square of the average inlet velocity:

$$k = \lambda \bar{u}^2, \tag{23}$$

where $\bar{u}$ is the average inlet velocity and λ is a percentage.

The dissipation is calculated according to the equation

$$\varepsilon = c_d \frac{k^{3/2}}{aD}, \tag{24}$$

where D is the inlet diameter. The values $\lambda = 0{\cdot}03$ and $a = 0{\cdot}005$ are commonly used and may vary slightly in the literature depending on the author.

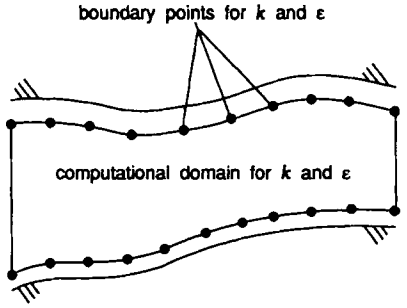

Figure 3. Calculation domain for law of the wall

Outlet. We suppose that the flow extends over a sufficiently long domain so that it is fully developed at the exit section. Thus for any variable ϕ the condition is

$$\frac{\partial \phi}{\partial x}=0. \tag{25}$$

Symmetry axis. Here the radial derivative of the variables is set equal to zero:

$$\frac{\partial \phi}{\partial r}=0. \tag{26}$$

3.2. *Boundary Conditions for the Vorticity and Streamfunction*

Solid walls

Laminar flow

When working with the vorticity–streamfunction formulation, there is no explicit Dirichlet-type boundary condition such as a zero velocity at walls imposed to satisfy the no-slip condition. The value of ω to be imposed is implicit because it depends on the flow itself. Moreover, it is the vorticity which is produced on solid walls which affects the flow field and which therefore has to be computed with care. In general[9] its value on solid walls is deduced from a Taylor series expansion of the streamfunction ψ around the solid point.

Let P be a point located at a distance Y_P from a wall point W and consider a local co-ordinate system X_W and Y_W where the direction given by Y_W is perpendicular to the wall (Figure 4).

Then a first-order boundary condition for the vorticity on solid walls which is also valid for variable density flows is given by[7,9]

$$\omega_W=\frac{2(\psi_W-\psi_P)}{Y_P^2 r_W \rho} \tag{27}$$

and a second-order boundary condition by

$$\left.\frac{\partial \omega}{\partial Y_W}\right|_W=\frac{6(\psi_W-\psi_P)}{r_W \rho Y_P^3}-3\frac{\omega_W}{Y_P}, \tag{28}$$

which now becomes a condition of the Neumann type. Equation (28) can further be worked by expressing the derivative in terms of backward differences. Thus

$$\omega_W=-\left(\frac{3(\psi_P-\psi_W)}{r_W \rho Y_P^2}+\frac{\omega_P}{2}\right). \tag{29}$$

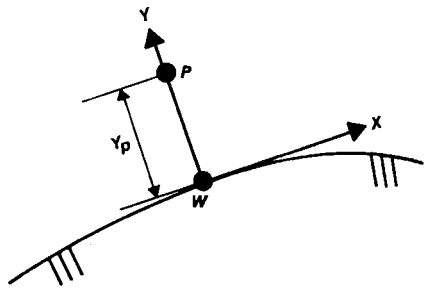

Figure 4. Calculation of vorticity at solid walls

Because of the small Y_P required by the turbulence resolution, the superiority of the second-order form was not evident in this work. Indeed, for the test cases to be presented here, no major differences were detected in the computed velocity field using (27) or (28). Because of its greater simplicity, we then adopted a first-order boundary condition.

For the streamfunction we impose a constant value on the walls because they are also streamlines. In order to find this value, the velocity profile can be integrated at a section where it is known (inlet) and the value of ψ can be fixed on another boundary (symmetry axis or solid). This allows the integration constant to be calculated. The condition for ψ on solid walls is therefore of the explicit Dirichlet type. This is not the case if the domain is multiply connected. Under these circumstances, for solid boundaries which are also obstacles (closed contours), the value of ψ has to be computed in another way.[16,17]

Turbulent flow

For turbulent flows the calculation of the streamfunction remains the same as before. The condition for the vorticity changes only when the law of the wall is used. In this case we must find a way to impose the shear stress τ_w at the wall according to the logarithmic distribution of the velocity close to the wall.

In order to do this, we must first recall that the mesh point adjacent to the wall is in the turbulent sublayer (Figure 2) and see how the law of the wall can be enforced when the (u, v, p) formulation is used. If the expression τ_w remains in the formulation and in the discretization, then its value can simply be computed from (17) knowing the friction velocity from (16). If not, a well known alternative is to compute a fictitious slip velocity on the wall. This is deduced from the logarithmic variation as follows.

First, equation (16) is derived with respect to y_p:

$$\frac{\partial U}{\partial y}=\frac{u^*}{\kappa y_p}. \tag{30}$$

Then, at point P and using backward difference, the derivative $\partial U/\partial y$ is evaluated:

$$\left.\frac{\partial U}{\partial y}\right|_P=\frac{U_P-U_W}{y_p}=\frac{u^*}{ky_p}. \tag{31}$$

Finally, the slip velocity U_W is given by

$$U_W=\begin{cases} U_P+u^*/\kappa & \text{if } U_P<0, \\ U_P-u^*/\kappa & \text{if } U_P>0, \end{cases} \tag{32}$$

and it has the same sign as U_P.

Given this slip velocity, we now have to modify the calculation of the vorticity on solid walls by reworking (27) or (28) without using $U_W=0$ on solid walls. For a first-order development we get an implicit Dirichlet-type boundary condition of the form (neglecting curvature effects)

$$\tfrac{1}{2}\,Y_P^2 r_W \rho\omega=\psi_W-\psi_P+r_W\rho U_W Y_P. \tag{33}$$

U_W is the local slip velocity relative to the frame illustrated in Figure 4 and computed from (32).

Inlet. At the inlet the velocity is known, so that the streamfunction and vorticity distributions are calculated from their own definitions (1) and (2).

Outlet. Conditions are the same as for k or ε, whether for ψ or ω (equation (25)).

Symmetry axis. The streamfunction is assigned a fixed value, while the vorticity ω is equal to zero because of the conditions $\partial u/\partial y=0$ and $v=0$ on the axis.

We conclude this section on boundary conditions by reiterating that in this work wall effects, when employing the k–ε model, are taken into account by a low-Reynolds-number model or by the law of the wall. This law is applied via the computation of a wall slip velocity and the corresponding vorticity.

4. THE NUMERICAL SOLUTION

In order to solve the set of partial differential equations previously described, the control-volume-based finite element technique presented by Baliga and Patankar[2] has been followed. Each equation in the system can have the following generic form

$$\frac{\partial}{\partial x}(\rho u\phi)+\frac{\partial}{\partial y}(\rho v\phi)=\frac{\partial}{\partial x}\left(\Gamma\frac{\partial\phi}{\partial x}\right)+\frac{\partial}{\partial y}\left(\Gamma\frac{\partial\phi}{\partial y}\right)+S_\phi, \tag{34}$$

where ϕ represents the scalar which undergoes convection and is diffused through the field, Γ is the exchange coefficient and S_ϕ is a source or sink term. A description of the discretization method by reference to this general transport equation follows. More details may be found in References 2, 18 and 4.

4.1. Domain discretization and interpolation function

The domain of interest is first divided into three-node triangular elements. Around the computational point P a control volume is created by joining the centroids of all neighbouring elements through the midpoints of the corresponding sides (Figure 5).

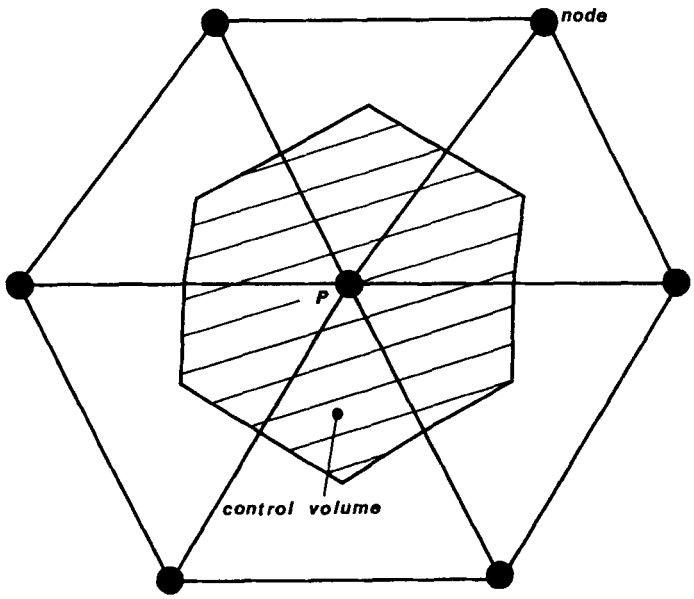

Figure 5. Polygonal control volume

Following the finite volume framework, equation (34) is integrated over the control volume. This procedure requires an interpolation function for ϕ. Baliga and Patankar[2] developed an approach based on the idea of using the exact solution of the one-dimensional convection–diffusion equation as the interpolation function, namely the exponential scheme first proposed by Allen and Southwell.[19] As an extension, an interpolation function that is as close as possible to the exact solution of the two-dimensional convection–diffusion equation was introduced. With the origin located at the centroid of the element, a locally flow-oriented co-ordinate system is defined ((X, Y), Figure 6). For each triangular element the interpolation function for ϕ is given by

$$\phi = AZ + BY + C, \tag{35}$$

with

$$Z = \frac{\Gamma}{\rho U_{av}} \left[\exp\left(\frac{\rho U_{av}(X - X_{max})}{\Gamma} \right) - 1 \right], \tag{36}$$

where X and Y are and local co-ordinates and $X_{max} = \max(X_1, X_2, X_3)$. U_{av} is the average local velocity component and is given by

$$U_{av} = (u_{av}^2 + v_{av}^2)^{1/2}, \tag{37}$$

where

$$u_{av} = \frac{u_1 + u_2 + u_3}{3}, \qquad v_{av} = \frac{v_1 + v_2 + v_3}{3}.$$

Γ and ρ are average values of the exchange coefficient and the density respectively that prevail over the element. The values of A, B and C are uniquely determined by the values of ϕ pertaining to the three nodes 1, 2 and 3.

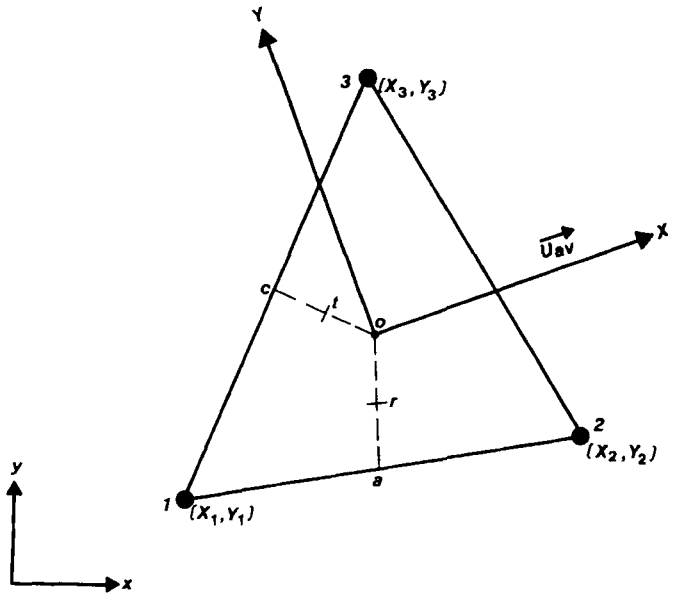

Figure 6. Triangular element with global (x, y) system and local (X, Y) flow-oriented co-ordinate system and related nomenclature

The good characteristics of this shape function have been further demonstrated by Prakash and Patankar[3] and Hookey and Baliga[4,20] for fluid flow or heat transfer problems using the primitive variable formulation or the vorticity–streamfunction formulation.[5] It must be pointed out that because there are no convection terms in the partial differential equation for the streamfunction ψ, the interpolation function for this variable is bilinear and given by $\psi = ax + by + c$. The resulting numerical scheme is then applied to solve laminar or turbulent incompressible flows.

One must add that the main advantage of an unstructured mesh-based control volume method, whether the elements are triangles or polygons, is the flexibility by which geometric complexity can be handled. Also, for the present two-dimensional applications the triangular discretization will lead to a matrix with a complicated sparsity pattern compared to a regular banded matrix arising from structured grids. However, this does not necessarily imply an excessive price to pay. If, for example, conjugate gradients-like methods combined with ILU preconditioning are used, the impact of the irregular node numbering does not decrease substantially the efficiency of these methods.[21] Therefore, although those solution procedures are not used here and the flow configurations simulated in this work do not contain fine geometrical details that require triangular unstructured meshes, because of its generality we used the unstructured mesh approach.

4.2. Discretized equations

The discretization of the equations is carried out by integrating (34) over the defined control volume. Using Simpson's rule through points a–r–o or o–t–c (Figure 6) and applying the divergence theorem, an equation of the form

$$a_p \phi_p + \sum a_{nb} \phi_{nb} = d_p \tag{38}$$

is obtained for each computational point, where a_p, a_{nb} and d_p are called the discretization coefficients,[4] subscript 'nb' refers to neighbouring points and subscript 'p' stands for the computational point P.

4.3. Boundary nodes and source terms

Boundary nodes. For nodes at Dirichlet boundaries, $a_p = 1$, $a_{nb} = 0$ and d_p becomes the known value of ϕ. For Neumann boundaries an equation of type (38) for each point of the boundary has to be written. We present here a convenient way of doing this for unstructured meshes.

Consider the boundary point W together with the triangle containing the normal to the boundary at that point and suppose a linear variation of the property ϕ in that triangle. Then, in the local (X, Y) frame of Figure 7, ϕ has the form

$$\phi = AX + BY + C. \tag{39}$$

From (39) the normal derivative is easily evaluated. In fact

$$\frac{\partial \phi}{\partial Y} = B = \sum_{i=1}^{3} N_i \phi_i, \tag{40}$$

where N_i are the base functions associated with the linear interpolation function of ϕ in the triangle containing the normal. In terms of the local (X, Y) co-ordinates pertaining to nodes 1, 2 and 3 of Figure (7), the N_i are

$$N_1 = \frac{X_3 - X_2}{J_C}, \qquad N_2 = \frac{X_1 - X_3}{J_C}, \qquad N_3 = \frac{X_2 - X_1}{J_C}, \tag{41}$$

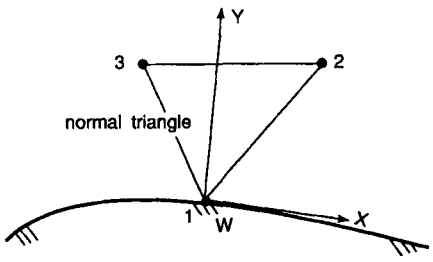

Figure 7. Boundary node and related nomenclature

where

$$J_C = |X_1(Y_2 - Y_3) - Y_1(X_2 - X_3) + X_2 Y_3 - X_3 Y_2|.$$

Thus, if the normal gradient is known from the boundary condition and Y is in the normal direction to the boundary, equation (40) is precisely of type (38) and therefore included in the global system. This is very useful when computations are done in a totally implicit way as is the case here.

Source terms. Source terms are integrated over the control volume (CV) by considering an average value calculated at the centroid and which prevails over the element, i.e.

$$\int_{CV} S \mathrm{d}V = \sum_{i=1}^{nb} \frac{S_i V_i}{3}, \tag{42}$$

where V_i is the volume (an area in 2D) of the element and the sum is taken over all the neighbours of the computational point.

Whenever it is possible, source terms are linearized so that the coefficient a_p may also include a part due to the linearization and discretization of the source term. However, for k and ε source terms special care was taken to avoid overshoots in the solution (negative values of k or ε). The procedure consisted of linearizing first the negative part of the source term and then including it in the discretization coefficient a_p on the left-hand side of (38). For a reason that will become apparent later, even if the remaining positive part of the source term can also be linearized and moved over to the left-hand side, it is kept on the right-hand side. The linearization of the negative part is done in the following way.

Let S_ϕ^- denote the negative part of the source term, ϕ being k or ε. S_ϕ^- may be written as

$$S_\phi^- = -\phi f(\phi), \tag{43}$$

where $f(\phi)$ is a function of ϕ. The linearization is then taken to be

$$(S_\phi^-)^{n+1} = -\phi^{n+1} f(\phi)^n, \tag{44}$$

where n stands for the value at the previous iteration.

This practice of taking the negative part only of the source term and including it on the left-hand side of (38) makes the resulting matrix more diagonally dominant and the iterative procedure converges. During the first iteration steps the values of k and ε still remain negative and after that they become admissible.

4.4. *Solution of the discretized equations*

For each computational point one equation of type (38) is written. These equations are then assembled to solve the entire field implicitly. The resulting matrix is sparse and without any particular structure and there are a number of suitable methods to solve the discretized equations. We used a sparse matrix solver from IBM's ESSL library.[22] The overall solution procedure can be outlined as follows.

1. Guess all the necessary variables.
2. If the law of the wall is used, then compute the slip velocity and boundary conditions for k–ε.
3. Solve the streamfunction–vorticity transport equations.
4. Solve the transport equations for k–ε.
5. Update the turbulent viscosity.
6. Treat the updated values of all variables as improved guesses and return to step 2 and repeat the process until convergence.

4.5. *Coupled or segregated?*

The transport equations for ω and ψ can be computed via direct coupling, i.e. considering ψ and ω as unknowns in a linear algebraic system of equations, or solved sequentially, first for ψ and then for ω. The latter requires less memory space.

Our numerical experiments showed that when solving for ψ and ω following a segregated approach, heavy underrelaxation was needed for both variables and convergence was slowed down especially at high Reynolds numbers. This can be attributed to the linear wall vorticity terms. In the coupled approach those terms are treated implicitly so that no underrelaxation is necessary and the procedure is rather insensitive to parameters such as the Reynolds number, thereby yielding a much more stable and robust procedure and a quicker convergence history as well. Thus the coupled approach has been used for all the numerical results to be presented below.

5. NUMERICAL RESULTS

The procedure and the method described above were applied to solve the following test cases:

(1) laminar axisymmetric flow in a channel with sudden contraction
(2) turbulent axisymmetric flow in a channel
(3) turbulent axisymmetric flow in a diffuser.

All the test cases are accompanied by experimental or analytical data from the literature that will be used to assess the validity and accuracy of the method. Meshes were generated using TRIA-2D.[23]

5.1. *Laminar flow in a pipe with sudden contraction of cross-sectional area*

This test has been chosen to investigate the validity of the scheme when applied to axisymmetric computations. It has been studied experimentally[24] and its global features are given in Figure 8. At the inlet of the pipe a parabolic fully developed velocity profile is imposed with a Reynolds number (based on the average inlet velocity and diameter) of 196. Owing to the symmetry of the problem, the calculation domain is only half the physical one. The domain is discretized with 567 nodes and 1071 elements distributed as shown in Figure 9.

Figure 10 shows a comparison between the current numerical predictions and the experimental data[24] at the six locations shown in Figure 8. The agreement is very good at all stations.

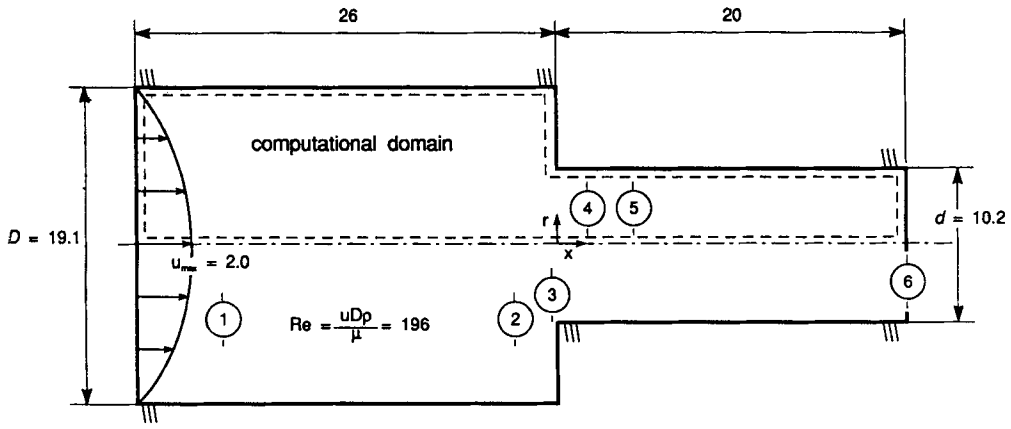

1. x/D = -1.047	4. x/d = 0.074
2. x/D = -0.157	5. x/d = 0.294
3. x/D = -0.039	6. x/d = 1.961

Figure 8. Global features of sudden contraction flow and location of comparison stations (scaled drawing)

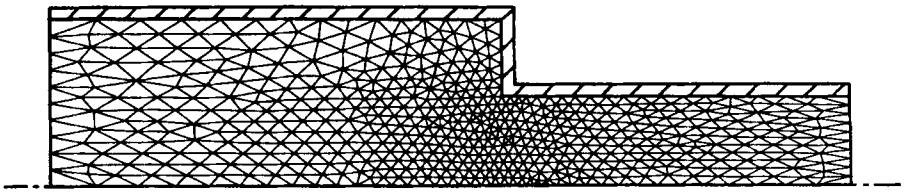

Figure 9. Domain discretization for sudden contraction flow, 567 nodes and 1071 elements

Convergence was reached after only 15 iterations using the coupled approach for a total CPU time of about 10 s on an IBM 3090 180 VF, giving approximately 1×10^{-3} s per iteration per point.

5.2. *Turbulent flow in a circular pipe*

Turbulent flow in a circular pipe is a classical and yet essential test for validating the setting of the turbulence model. We consider here a fluid that enters a circular channel with uniform velocity profile and a Reynolds number (based on average inlet velocity and diameter) equal to $1{\cdot}1 \times 10^5$ (Figure 11). At the exit the flow is entirely developed and we want to predict the velocity profile at this station.

Figure 12 shows the comparison between our numerical and Nikuradse's quasi-analytical results.[10] Wall effects were taken into account via the law of the wall by computing a slip velocity. Correspondence of the results is seen to be excellent. Figure 13 shows the classical flat turbulent velocity profile at the exit section.

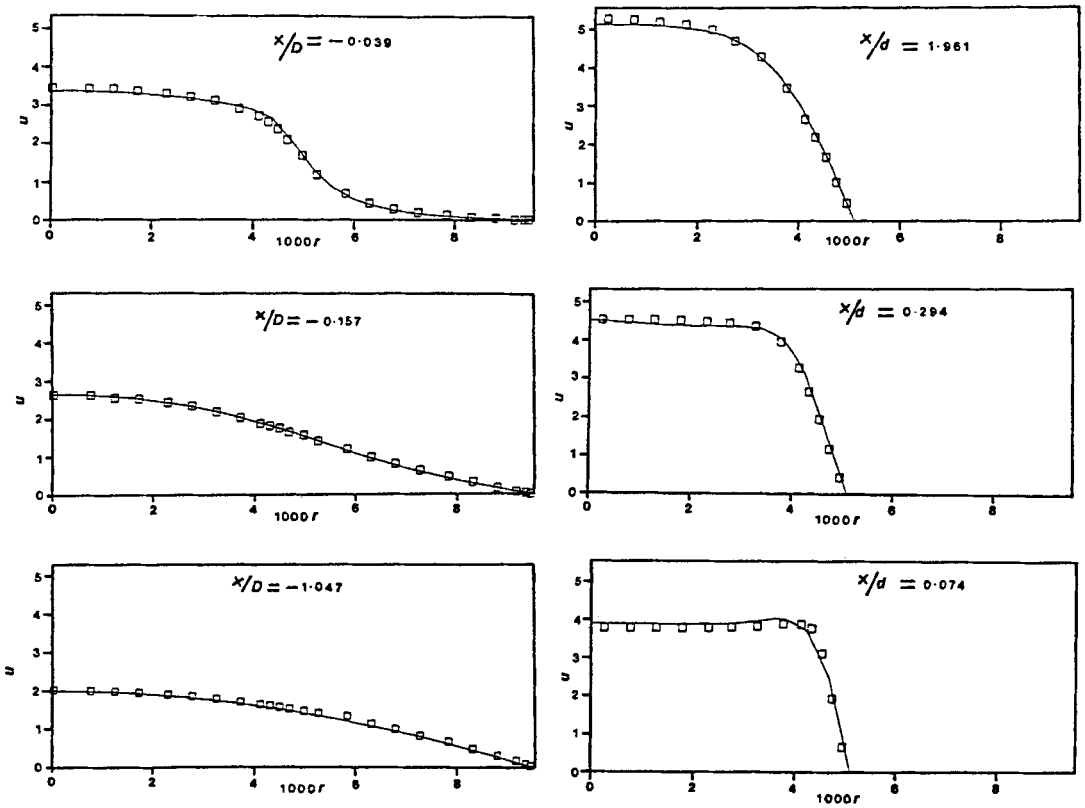

Figure 10. Comparison of measured (□, Reference 24) and predicted (——, present calculations) radial velocity distributions at various locations for sudden contraction flow

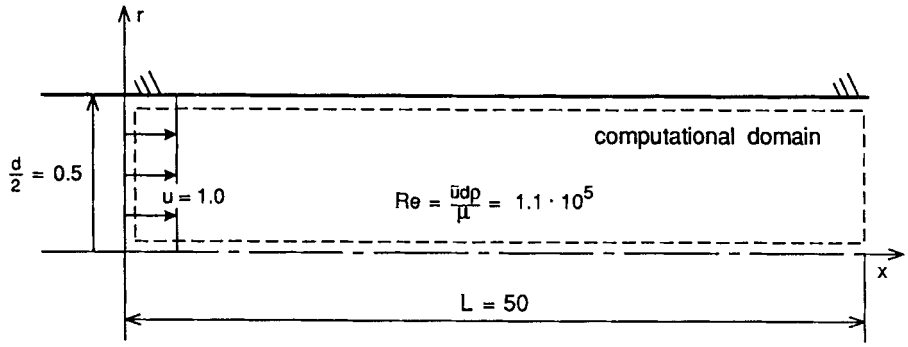

Figure 11. Global features of turbulent channel flow

The mesh consisted of 325 nodes and 576 elements. When the low-Reynolds-number model is used, results are of the same quality (not reported here); however, the total number of nodes (653) is higher and their distribution is more dense near solid boundaries. The computations, however, are more stable because of a different and more reliable boundary condition for the vorticity.

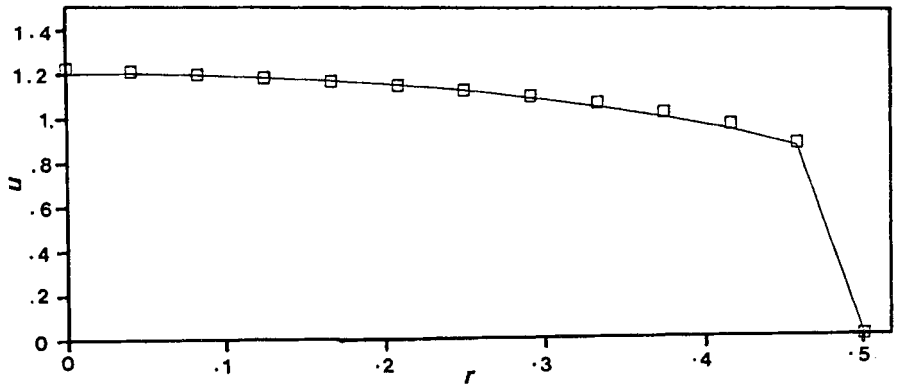

Figure 12. Developed velocity profile in circular channel turbulent flow: ——, present predictions with law of the wall; □, Reference 10

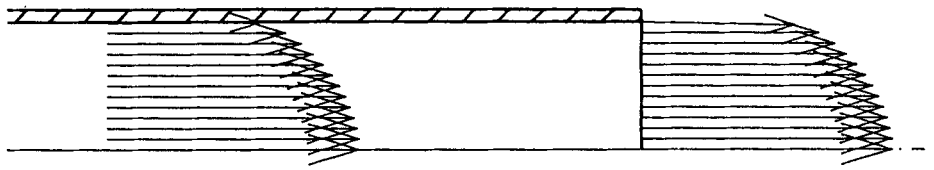

Figure 13. Flat velocity profile at circular channel exit

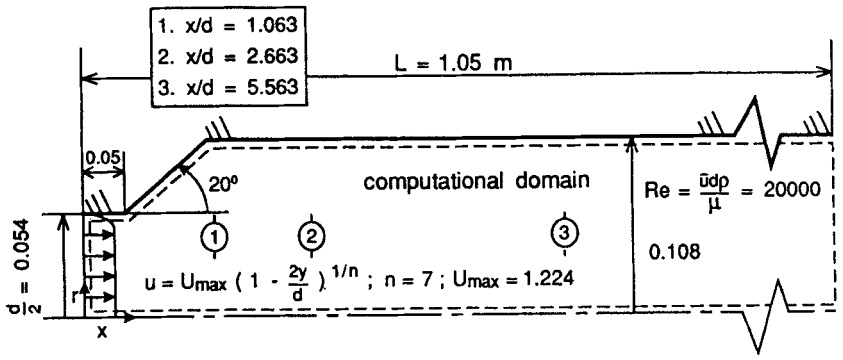

Figure 14. Global features of turbulent diffuser flow and location of comparison stations (scaled drawing in the x-direction)

5.3. Turbulent flow in a diffuser

This test case has been studied experimentally and numerically.[25] The general characteristics of this flow are given in Figure 14. The Reynolds number (based on the average inlet velocity and diameter) is equal to 2×10^4. Inlet conditions for k and ε are not known from the experimental data; in order to minimize their influence, we added a channel upstream so that the flow enters the diffuser with established profiles. Our numerical experiments showed that the results were sensitive to the entry level of turbulence when no channel was added upstream.

The results will be compared at three downstream stations (Figure 14), two of which are in the recirculation zone and the last one just after it. Also, in order to compare their performance, wall effects are included via the law of the wall or via the low-Reynolds-number model.

Results with the law of the wall. Figure 15 shows a comparison of the velocity profiles of our numerical predictions and the experimental data.[25] At the stations the predictions are only barely acceptable and are particularly bad close to the solid walls. Some recirculation region is still predicted but its intensity is too high and its length too short. Of course, predictions at the third station are strongly influenced by the predictions upstream and are therefore poor.

The mesh used here consisted of 615 nodes and 1120 elements and convergence was reached after 30 iterations. As described earlier, the special treatment of the source terms eliminated the problem of overshoots in the solution immediately after the first iterations.

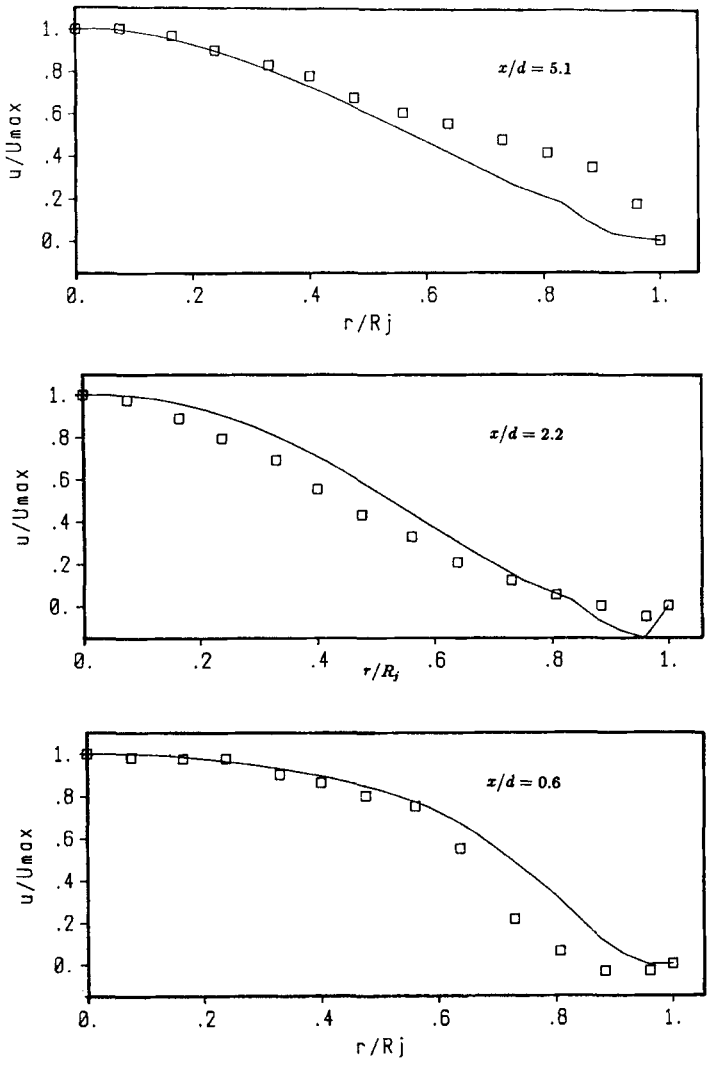

Figure 15. Velocity profiles at several stations, law of the wall: ——, present predictions; □, experimental data[25]

Results with the low-Reynolds-number model. In this case better predictions are obtained as illustrated in Figure 16. The size and intensity of the recirculation zone are now correct and at the last station the results are also better but to a lesser extent. In fact, the low-Reynolds-number model performs better in the recirculation region because the velocity close to the wall does not have a logarithmic variation anyway. The recirculation zone shown in Figure 17 is in good agreement with the numerical and experimental data of Reference 25. Because of the characteristics of the low-Reynolds-number model, more points were added, mainly in the recirculation zone and close to the solid walls, resulting in a mesh containing 756 points instead of the 615 points there were previously. Predictions in this region then improved dramatically. For a global enhancement many more points are needed, both in the whole field and concentrated close to the

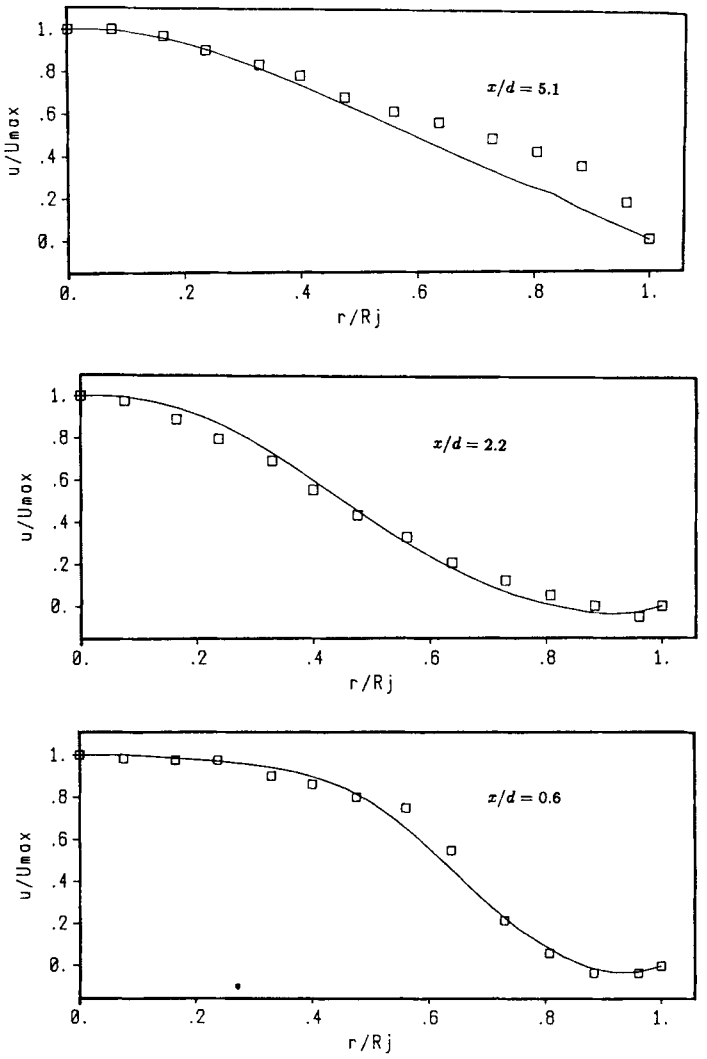

Figure 16. Velocity profiles at several stations, low-Reynolds-number model: ——, present predictions; □, experimental data[25]

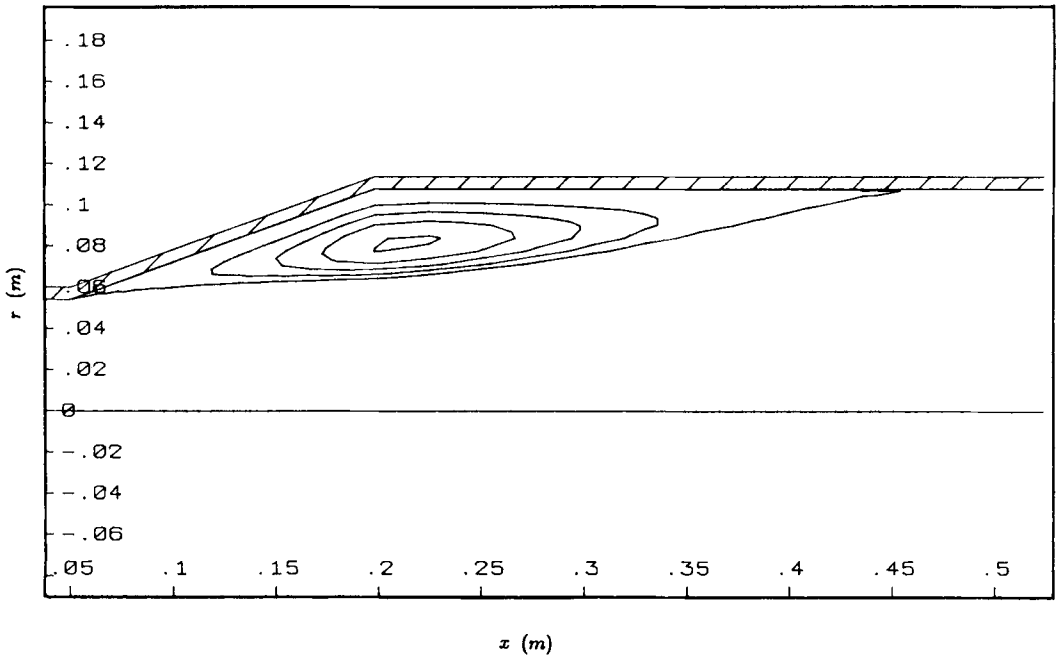

Figure 17. Streamlines in recirculation zone of turbulent diffuser flow

walls, as demonstrated by the channel flow test case and by the predictions at the third station, which are still poor.

6. CONCLUSIONS

A numerical procedure has been developed to solve laminar and turbulent flows. The study addressed the fluid flow problem via the vorticity–streamfunction formulation and used the standard k–ε equations for modelling the turbulence. Wall effects in turbulent flows were taken into account by a low-Reynolds-number model or by the use of the law of the wall and a suitable boundary condition for the vorticity. The method made use of the control-volume-based finite element method introduced by Baliga and Patankar.[2] The resulting discretized equations for the vorticity and streamfunction were solved in a coupled way to produce a fast and stable flow solver. Also, the special treatment of the source terms made it possible to avoid overshoots in the overall computations. Simulation of turbulent incompressible flows was found to be more accurate in the recirculating regions if a low-Reynolds-number model was used without requiring many more mesh points. However, for developed flows the law of the wall is more economical in terms of computing time and memory space (because fewer mesh points are needed for good predictions). The difficulties unique to the vorticity–streamfunction formulation and the low-Reynolds-number model are ones of stability because of the boundary condition on the vorticity that includes a fictitious slip velocity.

ACKNOWLEDGEMENTS

The authors acknowledge the financial support provided for this research by the CRIM (Centre de Recherche Informatique de Montréal), the FP (Fondation de Polytechnique), Gaz Métropolitain of Québec and the NRCC (National Research Council Canada).

REFERENCES

1. S. V. Patankar, *Numerical Heat Transfer and Fluid Flow*, Hemisphere/McGraw-Hill, New York, 1980.
2. B. R. Baliga and S. V. Patankar, 'A new finite-element formulation for convection–diffusion problems', *Numer. Heat Transfer*, **3**, 393–409 (1980).
3. C. Prakash and S. V. Patankar, 'A control volume-based finite element method for solving the Navier–Stokes equations using equal-order velocity–pressure interpolation', *Numer. Heat Transfer*, **8**, 259–280 (1985).
4. N. A. Hookey and B. R. Baliga, 'Evaluation and enhancements of some control volume finite-element methods—Part 1. Convection–diffusion problems', *Numer. Heat Transfer*, **14**, 255–272 (1988).
5. C. F. Kettleborough, S. R. Husain and C. Prakash, 'Solution of fluid flow problems with the vorticity–streamfunction formulation and the control-volume-based finite-element method', *Numer. Heat Transfer B*, **16**, 31–58 (1989).
6. C. Liu and S. McCormick, 'The finite volume-element method (FVE) for planar cavity flow', *Proc. 11th Int. Conf. on Numerical Methods in Fluid Dynamics*, Williamsburg, VA, June–July 1988, pp. 374–378.
7. A. D. Gosman, W. M. Pun, A. K. Runchal, D. B. Spalding and M. Wolfshtein, *Heat and Mass Transfer in Recirculating Flow*, Academic, London/New York, 1969.
8. W. P. Jones and B. E. Launder, 'The prediction of laminarization with a two-equation model of turbulence', *Int. J. Heat Mass Transfer*, **15**, 301–314 (1972).
9. P. J. Roache, *Computational Fluid Dynamics*, Hermosa, Albuquerque, NM, 1974.
10. H. Schlichting, *Boundary Layer Theory*, 7th edn, McGraw-Hill, New York, 1979.
11. R. S. Amano, 'Development of a turbulence near-wall model and its application to separated and reattached flows', *Numer. Heat. Transfer*, **7**, 59–75 (1984).
12. L. Martinelli and V. Yakhot, 'Turbulence transport approximations with applications to transonic flows', *Proc. AIAA 9th Computational Fluid Dynamics Conf.*, Buffalo, NY, June 1988, p. 221.
13. V. C. Patel, W. Rodi and G. Scheuerer, 'Turbulence models for near-wall and low Reynolds number flows: a review', *AIAA J.*, **23**, 1308 (1980).
14. C. C. Chieng and B. E. Launder, 'On the calculation of turbulent heat transport downstream from an abrupt pipe expansion', *Numer. Heat Transfer*, **3**, 189–207 (1980).
15. W. P. Jones and B. E. Launder, 'Predictions of low Reynolds number phenomena with a two-equation model of turbulence', *Int. J. Heat Mass Transfer*, **16**, 1119 (1973).
16. T. E. Tezduyar, R. Glowinski and J. Liou, 'Petrov–Galerkin methods on multiply connected domains for the vorticity–streamfunction formulation of the incompressible Navier–Stokes equations', *Int. j. numer. methods fluids*, **8**, 1269–1290 (1988).
17. M. D. Gunzburger and J. S. Peterson, 'On finite element approximation of the streamfunction–vorticity and velocity–vorticity equations', *Int. j. numer. methods fluids*, **8**, 1229–1240 (1988).
18. B. R. Baliga and S. V. Patankar, 'A control volume-based finite element method for two-dimensional fluid flow and heat transfer', *Numer. Heat Transfer*, **3**, 245–261 (1983).
19. D. N. Allen and R. V. Southwell, 'Relaxation methods applied to determine the motion, in two dimensions, of a viscous fluid past a fixed cylinder', *Q. J. Mech. Appl. Math.*, **8**, 129–145 (1985).
20. N. A. Hookey and B. R. Baliga, 'Evaluation and enhancements of some control volume finite-element methods—Part 2. Incompressible fluid flow problems', *Numer. Heat Transfer*, **14**, 273–293 (1988).
21. H. P. Langtangen, 'Conjugate gradient methods and ILU preconditioning of non-symmetric matrix systems with arbitrary sparsity patterns', *Int. j. numer. methods fluids*, **9**, 213–233 (1989).
22. *Engineering and Scientific Subroutine Library*, 4th edn, IBM, New York, 1983.
23. J. F. Hétu and D. Pelletier, 'Adaptive remeshing for viscous incompressible flows', *Proc. AIAA 21st Fluid Dynamics, Plasma Dynamics and Lasers Conf.*, Seattle, WA, June 1990.
24. F. Durst and T. Loy, 'Investigation of laminar flow in a pipe with sudden contraction of cross sectional area', *Comput. Fluids*, **13**, 15–36 (1985).
25. M. A. Habib and J. H. Whitelaw, 'The calculation of turbulent flow in wide-angle diffusers', *Numer. Heat Transfer*, **5**, 145–164 (1982).